Design of metal cofactors activated by a protein–protein electron transfer system

Takafumi Ueno*, Norihiko Yokoi†, Masaki Unno‡, Toshitaka Matsui‡, Yuichi Tokita§, Masako Yamada†, Masao Ikeda-Saito‡, Hiroshi Nakajima†, and Yoshihito Watanabe†¶

*Research Center for Materials Science and †Department of Chemistry, Graduate School of Science, Nagoya University, Furo-cho, Chikusa-ku, Nagoya 464-8602, Japan; ‡Institute of Multidisciplinary Research for Advanced Materials, Tohoku University, Katahira, Aoba, Sendai 980-8577, Japan; and §Materials Laboratories, Bio Electronics Laboratory Group 1, Sony Corporation, Atsugi Tec. No. 2 4-16-1 Okata Atsugi-shi, Kanagawa 243-0021, Japan

Edited by Jay R. Winkler, California Institute of Technology, Pasadena, CA, and accepted by the Editorial Board May 8, 2006 (received for review December 19, 2005)

Protein-to-protein electron transfer (ET) is a critical process in biological chemistry for which fundamental understanding is expected to provide a wealth of applications in biotechnology. Investigations of protein–protein ET systems in reductive activation of artificial cofactors introduced into proteins remains particularly challenging because of the complexity of interactions between the cofactor and the system contributing to ET. In this work, we construct an artificial protein–protein ET system, using heme oxygenase (HO), which is known to catalyze the conversion of heme to biliverdin. HO uses electrons provided from NADPH/cytochrome P450 reductase (CPR) through protein–protein complex formation during the enzymatic reaction. We report that a Fe^{III}(Schiff-base), in the place of the active-site heme prosthetic group of HO, can be reduced by NADPH/CPR. The crystal structure of the Fe(10-CH_2CH_2COOH-Schiff-base)·HO composite indicates the presence of a hydrogen bond between the propionic acid carboxyl group and Arg-177 of HO. Furthermore, the ET rate from NADPH/CPR to the composite is 3.5-fold faster than that of Fe(Schiff-base)·HO, although the redox potential of Fe(10-CH_2CH_2COOH-Schiff-base)·HO (−79 mV vs. NHE) is lower than that of Fe(Schiff-base)·HO (+15 mV vs. NHE), where NHE is normal hydrogen electrode. This work describes a synthetic metal complex activated by means of a protein–protein ET system, which has not previously been reported. Moreover, the result suggests the importance of the hydrogen bond for the ET reaction of HO. Our Fe(Schiff-base)·HO composite model system may provide insights with regard to design of ET biosystems for sensors, catalysts, and electronics devices.

heme oxygenase | metalloprotein | protein–protein interaction | schiff-base | hydrogen bond

Design of biological protein–protein electron transfer (ET) systems (1–6) for the creation of artificial catalysis and bioelectronics devices for novel biosensors is a challenging objective (7–9). Several researchers have made significant advances in construction of artificial ET biosystems by chemical modification of native cofactors (10–12), substrates (13), and enzymes (14). For example, Gray and Winkler (6) reported that synthetic light harvesting metal complexes bound to metalloproteins can act as triggers of ET reactions. However, challenges remain for introduction of unnatural molecules into protein scaffolds in design of ET systems because of the challenges in understanding the complex noncovalent interactions contributing to ET processes.

Heme oxygenase (HO) is known to catalyze the conversion of heme to biliverdin. HO utilizes electrons provided from a NADPH/cytochrome P450 reductase (CPR) system (Fig. 1*A*) (15). The first electron reduces the heme Fe(III) to Fe(II) to initiate the enzymatic reaction, which is followed by a second reduction of O_2-ligated heme for the hydroxylation of the C^{α} atom of the heme (Fig. 1*A*). The electron flow has been proposed to proceed from NADPH to the heme iron atom of the redox partner, HO, via the FAD and FMN domains of CPR (16). Furthermore, docking simulation of CPR and HO shows that HO binds to the FMN domain of CPR with the HO heme in close proximity to the FMN group (17). These observations suggest that an unnatural metal cofactor incorporated into the active site

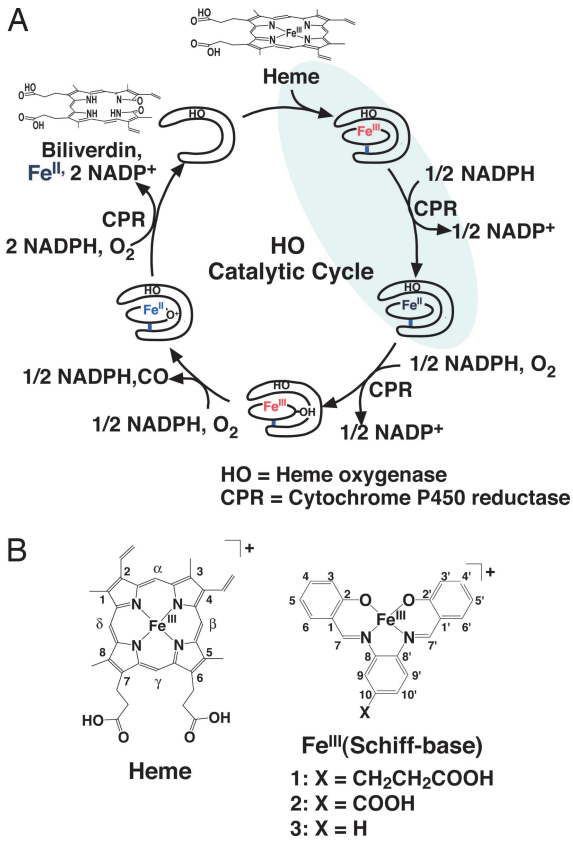

Fig. 1. Catalytic reaction of HO. (*A*) Enzymatic cycle of heme metabolism to biliverdin catalyzed by HO. The reactions shaded in blue indicate the ET step from CPR to heme to be used for the reduction of Fe^{III}(Schiff-base) complexes. (*B*) Chemical structures of heme (*Left*) and Fe^{III}(Schiff-base) (*Right*).

Conflict of interest statement: No conflicts declared.

This paper was submitted directly (Track II) to the PNAS office. J.R.W. is a guest editor invited by the Editorial Board.

Abbreviations: ET, electron transfer; CPR, cytochrome P450 reductase; HO, heme oxygenase.

Data deposition: The atomic coordinates have been deposited in the Protein Data Bank, www.pdb.org [PDB ID codes 1WZD (**1·HO**), 1WZF (**2·HO**), and 1WZG (**3·HO**)].

¶To whom correspondence should be addressed. E-mail: yoshi@nucc.cc.nagoya-u.ac.jp.

of HO may be capable of accepting electrons from NADPH through CPR.

We have previously reported the replacement of heme in myoglobin with Schiff-base complexes as a novel method for the introduction of synthetic metal cofactors into protein scaffolds (18–20). Importantly, the myoglobin crystal structures indicate that the Schiff-base complex in the heme cavity adopts an orientation similar to that of heme. In addition, stability and catalytic reactivity of the composites have been improved by modification of noncovalent interactions (19, 20). Here, we report the molecular design of a protein–protein ET system wherein electrons are transferred from NADPH/CPR to the Fe(Schiff-base) complex-reconstituted HO. Also reported are investigations of this system as a model for activation of unnatural metal cofactors in native protein–protein ET systems. The crystal structures of the composites show that the hydrogen bond between the Schiff-base ligand and Arg-177 in HO plays important roles in the ET reaction from NADPH/CPR to the Fe(III) ion reconstituted in HO. The results provide us with previously undescribed concepts for design of hybrid electronics devices employing protein–protein complexes with unnatural cofactors.

Results and Discussion

Design of Fe^{III}(Schiff-Base) Complexes. A Schiff-base ligand **1** was designed for reconstitution with HO as shown in Fig. 1*B*. The crystal structure of **heme·HO** shows that Arg-177 forms a hydrogen bond with the heme propionate-7 (Fig. 2*A*) (21). In general, the participation of heme propionates in hydrogen bonds with nearby residues provides stabilization of the heme-protein composites (22). Interestingly, the interactions are conserved in other HOs (23, 24) and are proposed to be important for the ET reaction with CPR (17). Thus, we have introduced a propionate group at the C10 of **1**, because the substituent in **1** is expected to interact with Arg-177 if His-20 ligates to the iron atom of **1**. For the comparison, we have also prepared **2**, in which a carboxylate group was introduced at the C10 position, and **3**, which has no substituent (Fig. 1*B*). The composites of the Schiff-base complexes and HO were reconstituted by using a modified method recently reported (18). Melting points (T_m) of the composites obtained from the temperature dependence of the CD spectra are 39.2, 34.1, and 33.4°C for **1·HO**, **2·HO**, and **3·HO**, respectively. The results suggest that the propionate in **1** is critical for improvement of the thermal stability of the composite.

Crystal Structures. The crystal structures of **1·HO**, **2·HO**, and **3·HO** have been refined to 1.35-, 1.85-, and 1.75-Å resolution, respectively (see *Supporting Text* and Table 4, which are published as supporting information on the PNAS web site). Two molecules exist in the asymmetric units of the crystals of each composite that can be superimposed with the root-mean-square (rms) deviations of backbone atoms of only 0.42, 0.44, and 0.42 Å for **1·HO**, **2·HO**, and **3·HO**, respectively. The rms deviations of **1·HO**, **2·HO**, and **3·HO** from **heme·HO** (21) are also only 0.54 (Fig. 3*A*), 0.56, and 0.55 Å, respectively. The small deviation suggests that the conformations and orientations of the composites are almost identical to that of the heme within HO. The electron density maps of the active sites of the composites are shown in Fig. 2 *B–D*. Although the Fe(Schiff-base) complex reconstituted into apo-Mb retains a planar structure by the ligation of axial His and a water molecule (19), Fe(III) in **1·HO** exhibits distorted octahedral coordination geometry (Fig. 2*B*). This structural perturbation in the active site of **1·HO** is due to weak ligation of Oε(Glu-24) to the iron at a distance of 2.16 Å and noncovalent interactions of **1** with Gly-135, Gly-139, Phe-201, Asn-204, and Phe-208 (close contacts within 4 Å; Fig. 3 *B* and *C*). These interactions are also observed in **2·HO** and **3·HO**, and the coordination geometries of **2** and **3** are almost identical to that

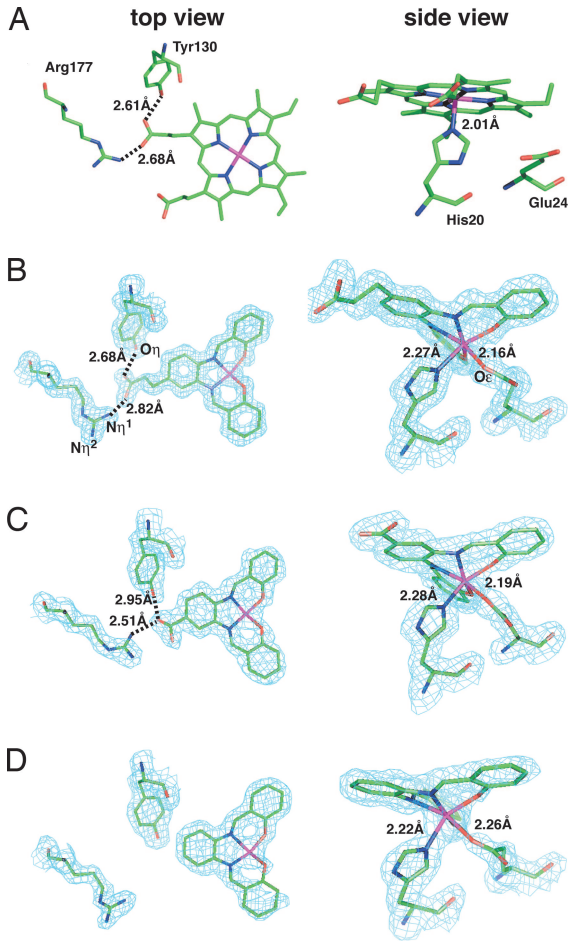

Fig. 2. Close-up views of coordination geometries of the metal cofactors in the HO active-site region. Refined model coordinates for the active site region are superimposed on $2F_o - F_c$ maps contoured at 1.0 σ, except for heme·HO, with elements of the protein and cofactors in ball-and-stick models for top (*Left*) and side (*Right*) views. Green is carbon, and purple, red, and pink are nitrogen, oxygen, and iron, respectively. (*A*) Heme·**HO**. (*B*) **1·HO** refined to 1.35 Å. (*C*) **2·HO** refined to 1.85 Å. (*D*) **3·HO** refined to 1.75 Å.

of **1** in **1·HO** (Fig. 2 *C* and *D*). Thus, ligation of the Oε(Glu-24) to the iron atom and the noncovalent interactions are important factors that determine both the position and geometry of the Fe(Schiff-base) complex in the active site. In addition, the position of **1** in HO is almost identical to that of the native heme (Fig. 3 *D* and *E*). During the reconstitution of apo-Mb with heme, two binding modes of the heme are observed at an early stage (25). Even for the heme·HO complex, a minor conformation has been reported in solution that is influenced by interactions of the two heme propionic acid groups (26). In contrast, there is only one carboxylic acid in **1** and **2**, making alternative binding modes unlikely to occur. With respect to the hydrogen bond of **1**, each oxygen atom of the propionic acid of **1** shows hydrogen bonds with Nη^1(Arg-177) and Oη(Tyr-130) (Fig. 2*B*) as observed in **heme·HO** (Fig. 2*A*) (21). On the other hand, one oxygen atom of the carboxyl group of **2** forms two hydrogen bonds with both of Nη^1(Arg-177) and Oη(Tyr-130), which have the effect of directing the guanidine group of Arg-177 toward inside of the cavity (Fig. 2*C*).

Fe(II)/Fe(III) Redox Potentials of Fe^{III}(Schiff-Base)·HO Composites. The redox potentials of **1·HO**, **2·HO**, and **3·HO** were determined by potentiometric titration using the UV-visible spectral changes and

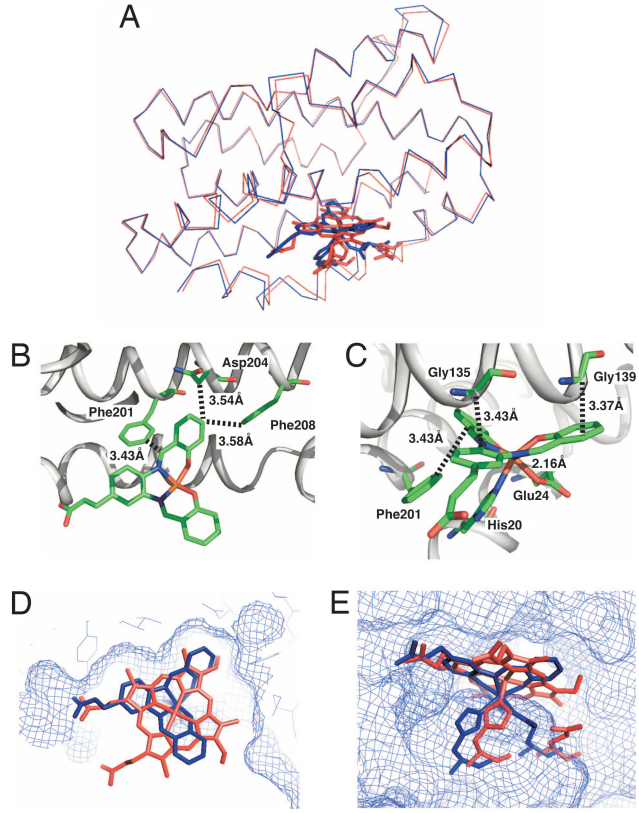

Fig. 3. Crystal structure of **1·HO**. (*A*) Overall structure of **1·HO** (blue) superimposed on **heme·HO** (red) with 0.54 Å of the backbone rms deviation. (*B*) A close-up view of noncovalent interactions of **1** with Phe-201, Asp-204, and Phe-208 in the active site. (*C*) A close-up view of noncovalent interactions of **1** with Gly-135, Gly-139, and Phe-201 in the active site. The closest contacts between the Schiff-base ligand and the residues are indicated by broken lines and the distances. (*D*) A top view of the active site of **1·HO** (blue) superimposed on **heme·HO** (red). (*E*) A side view of the active site of **1·HO** (blue) superimposed on **heme·HO** (red). Complex *1* (blue), heme (red), and the ligated His-20 in HOs are shown as tube models.

are listed in Table 1 (see Fig. 5, which is published as supporting information on the PNAS web site). The redox potential of **1·HO** determined from the Nernst plot of the spectral change was −76 mV vs. normal hydrogen electrode (NHE). The potentials of **2·HO** (−49 mV) and **3·HO** (15 mV) also were obtained from their

Table 1. Redox potentials and reduction rate constants of Fe^{III}(Schiff-base)·HO composites and heme·HO

Composite	Redox potential;* $E_{1/2}$, mV vs. NHE	Reduction rate constants: $Na_2S_2O_4$† k_1, $M^{-1/2}\cdot s^{-1}$	Reduction rate constants: NADPH/CPR‡ k_2, $mM^{-1}\cdot s^{-1}$
1·HO	−76 ± 5.3	108 ± 2.4	196 ± 3.7
2·HO	−49 ± 4.3	181 ± 4.0	148 ± 3.6
3·HO	15 ± 7.6	1036 ± 15	56.5 ± 1.8
Heme·HO	−65 ± 1§	490 ± 5.1	302 ± 21

All experiments were carried out in 10 mM Tris·HCl buffer (pH 7.4) at 15°C under an Ar atmosphere.
*[Fe(Schiff-base)·HO] = 300 μM, [NaCl] = 100 mM, and [electron mediator] = 5 μM. NHE, normal hydrogen electrode.
†[Fe(Schiff-base)·HO or heme·HO] = 5 μM, and [$Na_2S_2O_4$] = (100–2,000 μM).
‡[Fe(Schiff-base)·HO or heme·HO] = 5 μM, [CPR] = (0.5–3.0 μM), and [NADPH] = 100 μM.
§Ref. 27.

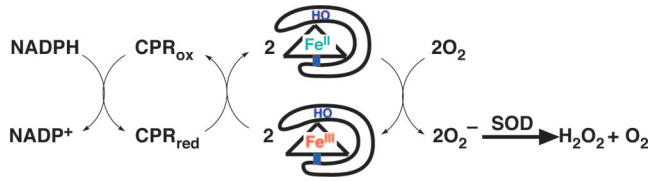

Fig. 4. Coupling reactions of NADPH consumption with CPR, O_2 reduction by Fe(Schiff-base)·HO composite, and superoxide dismutation by superoxide dismutase (SOD).

spectral changes. The trend is different from that of the metal complexes in *N*,*N*-dimethylformamide (DMF) [**2·Cl**(−16 mV) > **3·Cl**(−58 mV) > **1·Cl**(−59 mV) vs. NHE]. This result indicates that the midpoint potentials of **1·HO**, **2·HO**, and **3·HO** are influenced by the surrounding protein environment, rather than the substituent effect on the ligand (6). The redox potential of cytochrome *c* was reported to be influenced by charge contribution of the heme 7-propionate (28). Thus, we propose that the large negative redox potentials of Schiff-base complexes, **1** and **2**, in HO could arise from the negative charge of carboxylate. These potentials are higher than that of FMN in CPR (−288 mV) (29); thus, they are expected to accept one electron from NADPH via CPR.

Reduction Rates of Fe^{III}(Schiff-Base)·HO Composites. The reduction rates of **1·HO**, **2·HO**, **3·HO**, and **heme·HO** by sodium dithionite ($Na_2S_2O_4$) (k_1) and NADPH/CPR system (k_2) are listed in Table 1. The rate constant k_1 of **1·HO** (108 $M^{-1/2}\cdot s^{-1}$) is 1.7-fold and 9.6-fold less than those of **2·HO** (181 $M^{-1/2}\cdot s^{-1}$) and **3·HO** (1,036 $M^{-1/2}\cdot s^{-1}$), respectively. The values show a linear correlation of $E_{1/2}$ with respect to logk_1 (30). On the other hand, the rate constant k_2 of **1·HO** (196 $mM^{-1}\cdot s^{-1}$) is 1.3- and 3.5-fold larger than those of **2·HO** (148 $mM^{-1}\cdot s^{-1}$) and **3·HO** (56.5 $mM^{-1}\cdot s^{-1}$), respectively. This trend in k_2 is opposite to that of relative order of k_1. The k_1 and k_2 of **heme·HO** are larger than those of **1·HO** and **2·HO**. These results indicate that the active site of HO is more suitable for the redox reaction of heme than those of the Schiff-base complexes.

Catalytic O_2 Reduction by Fe^{III}(Schiff-Base)·HO Composites. To evaluate the effects of the hydrogen-bonding interaction on the catalytic ET reaction from NADPH to the iron atom, we monitored the rates of NADPH and O_2 consumption occurring in the catalytic reaction shown in Fig. 4. The rates at the initial stage are listed in Table 2. The reduced Fe(II) in **1·HO**, **2·HO**, and **3·HO** yields O_2^- by one electron oxidation of Fe(II) through the formation of an $Fe^{II}(O_2)$ complex (31). Unligated O_2^- readily disproportionates to O_2 and H_2O_2 in the presence of superoxide dismutase (SOD). H_2O_2 formation was detected by subtracting the oxygen consumption rate of **1·HO** in the absence of catalase

Table 2. Catalytic NADPH and O_2 consumption rate of Fe(Schiff-base)·HO composites and Fe(Schiff-base)·Cl complexes

Composite	−d[NADPH]/dt, μM·min^{-1}	−d[O_2]/dt, μM·min^{-1}	d[O_2]/d[NADPH]
1·HO	21 ± 1.2	21 ± 0.3	1.0
2·HO	18 ± 0.2	14 ± 0.6	0.78
3·HO	5.5 ± 0.2	5.1 ± 0.1	0.93
1·Cl	24 ± 1.9	4.8 ± 0.3	0.20
2·Cl	24 ± 0.6	11 ± 0.6	0.44
3·Cl	31 ± 2.5	12 ± 0.8	0.39
Blank*	0.14 ± 0.03	0.6 ± 0.1	—

Conditions: [Fe complex] = 2 μM, [NADPH] = 100 μM, [CPR] = 1 μM, and SOD = 100 units in 10 mM Tris·HCl buffer (pH 7.4) at 15°C under air.
*Same conditions, except for [Fe] = 0 μM.

from that determined in the presence of catalase and then multiplying the value by a factor of 2 (catalase reacts with 1 mol of H_2O_2 to generate 1/2 mol of O_2) (27). The NADPH consumption rate of **1·HO** (21 μM·min^{-1}) is 1.2- and 3.8-fold faster than the NADPH consumption rates of **2·HO** (18 μM·min^{-1}) and **3·HO** (5.5 μM·min^{-1}), respectively. Apparently, the reduction rates of **1·HO**, **2·HO**, and **3·HO** by NADPH/CPR (Table 1) correlate with consumption rates of O_2 but not with their redox potentials. Further, the rates of catalytic NADPH consumption and O_2 consumption are similar, indicating that the reduced Fe^{II}(Schiff-base) in HO efficiently reduces O_2 to O_2^-. These results indicate an important role of the hydrogen bonding that occurs between Arg-177 and the Schiff-base ligand (Fig. 2). On the other hand, the O_2 consumption rates of **1·Cl**, **2·Cl**, and **3·Cl** are 0.20, 0.44, and 0.39 times less, respectively, than their respective NADPH consumption rates. Decreased O_2 consumption suggests that the irreversible formation of μ-oxo dimer of Fe^{II}(Schiff-base) inhibits the catalytic reaction (32).

Role of the Hydrogen Bond on Arg-177. The thermal stability and redox reactions clearly indicate that the hydrogen bond of the Schiff-base ligand with Arg-177 influences the properties of the Fe(Schiff-base)·HO composites. Most interestingly, the order of reduction rate constants determined with NADPH/CPR (k_2) is opposite to those of the redox potentials and reduction rate constants determined with $Na_2S_2O_4$ (k_1) (Table 1). Crystal structures of human (23), rat (24), and *Corynebacterium diptheriae* (21) HOs indicate the presence of an invariant hydrogen bond between the guanido Nη^1 atom of Arg-177 (Arg-183 in human and rat HO) and the O atom of heme propionate-7 with the other Nη^2 atom exposed to the solvent (21). Experiments with Arg-177 deleted mutants indicated that Arg-177 contributes significantly to maintaining the proper orientation of the heme within the active site and preserving the catalytic turnover of heme decomposition in the CPR catalyzed reaction (26, 33). Further, Arg-177 has been identified as one of the most important residues for preserving the electrostatic interaction of the transient ET complex with CPR (17). Thus, the exposed Nη^2 atom of Arg-177 is expected to play dual roles in binding and ET with CPR in a manner similar to that suggested for Arg-112 in P450cam (34). In the case of Fe(Schiff-base)·HOs, **1** retains the hydrogen bond with Arg-177 (Fig. 2 *A* and *B*), indicating that **1** is capable of receiving an electron from CPR. On the other hand, Arg-177 in **2·HO** is not exposed to the solvent because one oxygen atom of the carboxyl group of **2** forms two hydrogen bonds with Nη^1(Arg-177) and Oη(Tyr-130) (Fig. 2*C*), and **3** is lacking a hydrogen bond with Arg-177 (Fig. 2*D*). Thus, Arg-177 in **2·HO** and **3·HO** is expected to exhibit less of an effect on the ET reaction with CPR than that of **1·HO**. The k_2 data showing the order of **1·HO** $\sim$ **2·HO** $>$ **3·HO** are consistent with these considerations (Table 1).

Unrestricted Hartree–Fock calculations were carried out to elucidate the contribution of the hydrogen bond to the redox reactions. The electronic states of Fe(III) and Fe(II) of **1·HO**, **2·HO**, and **3·HO** were assumed to be high-spin (sextet) and low-spin (singlet), respectively. We used the coordination geometry of the Fe(Schiff-base), His-20, Asp-24, Tyr-130, and Arg-177 from the crystal structures as the fixed models. The calculated energy differences [$\Delta E_{(Fe(II)\text{-}Fe(III))}$] between both states of each model show the order of **1·HO** (61.6 kcal/mol) $>$ **2·HO** (52.8 kcal/mol) $>$ **3·HO** (15.9 kcal/mol). The results are consistent with the trend observed for the Fe(II)/Fe(III) redox potentials (Table 1). If it is assumed that the electron from NADPH/CPR is transferred the to Fe^{III}(Schiff-base) through hydrogen bonding with Arg-177, the unoccupied β orbital of Arg-177 should be used to accept an electron from CPR with concomitant decrease in the energy level of the occupied orbital to the level of the α orbital. However, we cannot compare the electron affinities of each Fe(III) model obtained from Koopmans' theorem (35) because they have different total charges. Thus, the efficiency of the hydrogen bond with Arg-177 on the ET reaction was estimated by using $\Delta E_{(\beta\text{-}\alpha)}$. Table 3 shows the energy values of the β orbitals on Arg-177 and the corresponding α orbitals. The trend in the energy difference between the α and β orbital is **1·HO** $>$ **2·HO** $>$ **3·HO** (Table 3). These results suggest that the electron used to reduce Fe(III) in **1·HO** is transferred from CPR to Arg-177 at a rate that is faster than the analogous rates for **2·HO** and **3·HO**. In fact, the reduction rate of **1·HO** by NADPH/CPR is greater than those of **2·HO** and **3·HO**. The experimental and theoretical results indicate that consideration of efficient ET is a very important characteristic for design of efficient artificial redox centers to be introduced into protein scaffolds.

Table 3. Selected α and β orbital energy values calculated for Fe^{III}(Schiff-base)·HO models

Composite	MOs	E_β, kcal/mol	E_α, kcal/mol	$\Delta E_{(\beta-\alpha)}$, kcal/mol
1·HO	273 (LUMO + 2)	55.2	−191	246
	274 (LUMO + 3)	57.6	−181	239
2·HO	265 (LUMO + 2)	53.3	−188	241
	267 (LUMO + 4)	63.3	−166	229
3·HO	252 (LUMO)	−16.9	−234	217
	255 (LUMO + 3)	6.91	−218	225
	256 (LUMO + 4)	11.9	−204	216

MO, molecular orbital; LUMO, lowest unoccupied MO.

In summary, this study provides a previously undescribed approach for regulation of ET reactions of synthetic metal complexes by taking advantage of the process of protein–protein complex formation of native ET biosystems. In particular, we have succeeded in fixing and reductively activating our Fe(Schiff-base) complexes in HO by using the hydrogen bond conserved within the native enzymatic system. Hydrogen-bonding and noncovalent interactions are also important in ET reactions of metalloproteins (4–6, 34, 36). The results therefore suggest that ET properties of synthetic molecules in native biosystems could be regulated if they are designed to retain the conserved interactions in proteins. This approach may represent a significant advance toward the development of bioelectronics systems capable of activating or regulating numerous functions of synthetic molecules for biomedical and electronics applications.

Materials and Methods

Preparation of Fe^{III}(Schiff-Base)·HO Composites. The procedures for expression and purification of HO from *Corynebacterium diotheriae* were performed as described in ref. 15. Syntheses of Fe[*N*, *N*′-bis(salicylidene)-3,4-diamino benzenepropanoic acid]·**Cl** (**1·Cl**), Fe[*N*, *N*′-bis(salicylidene)-3,4-diamino benzoic acid]·**Cl** (**2·Cl**), and Fe[*N*, *N*′-bis(salicylidene)-phenylenediamine] (**3·Cl**) are described in *Supporting Text*. To a dimethylformamide (DMF) (1 ml) solution of **1·Cl** (11.2 mg, 25 μmol) was added $AgBF_4$ (4.8 mg, 25 μmol), and the mixture was refluxed for 6 h, after which AgCl was precipitated and removed by celite filtration. The diluted solution (4 mM, 300 μl) was slowly added to an aqueous solution of HO (100 μM, 10 ml of 10 mM Tris·HCl buffer, pH 7.4) and gently stirred at 4°C for 30 min. The mixture was dialyzed against 10 mM Tris·HCl (pH 7.4) overnight at 4°C. After dialysis, the mixture was passed through Sephadex G25 (10 mM Tris·HCl buffer, pH 7.4). The composite was purified by DE52 (Whatman) and HiTrapQ (Amersham Pharmacia Biosciences) columns with linear gradients of potassium chloride (0–0.4 M) in 10 mM Tris·HCl buffer (pH 7.4). UV/Vis: λ_{max} 417 nm (ε/m^{-1}·cm^{-1} 9,500), 365 nm (19,500), 328 nm (28,000), 282

CHEMISTRY

nm (60,000); MS (ESI-TOF): (m/z)z calculated for **1·HO** $[M]^-$, 24,427.5; found, 24,435.5 ± 3.0. **2·HO** and **3·HO** were synthesized and purified by the same procedure. **2·HO**: UV/Vis: λ_{max} 425 nm ($\varepsilon/m^{-1}\cdot cm^{-1}$ 8,000), 365 nm (17,500), 325 nm (25,000), 281 nm (61,000); MS (ESI-TOF): (m/z)z calculated for **2·HO** $[M]^-$, 24,399.5; found, 24,396.1 ± 4.5. **3·HO**: UV/Vis: λ_{max} 427 nm ($\varepsilon/m^{-1}\cdot cm^{-1}$ 10,000), 365 nm (21,000), 324 nm (30,000), 280 nm (73,500); MS (ESI-TOF): (m/z)z calculated for **3·HO** $[M]^-$, 24,355.5; found, 24,349.6 ± 5.4.

Determination of Reduction Rate Constant (k_1) by Sodium Dithionite ($Na_2S_2O_4$). The reduction rate constants (k_1) of Fe^{III}(Schiff-base)·HO composites to the Fe(II) composites were determined by a reported procedure (37). To obtain k_1, the observed pseudo-first-rate constants were fitted vs. $[Na_2S_2O_4]^{-1/2}$ as described (37) (see Figs. 6 and 7, which are published as supporting information on the PNAS web site). The pseudo-first-order rate constants were obtained from absorption changes at 400 nm after flush mixing of Fe(Schiff-base)·HO composites (final concentration: 5 μM) with $Na_2S_2O_4$ (final concentration: 100, 250, 500, 750, and 1,250 μM) in 10 mM Tris·HCl (pH 7.4) at 15°C. The spectra were recorded on a stopped-flow RSP601 (UNISOKU, Osaka).

Determination of Reduction Rate Constant (k_2) by NADPH/CPR. The reduction rate constants (k_2) of Fe(Schiff-base)·HOs were determined according to a previous report (38). Each k_2 was calculated from the slope of the observed pseudo-first-order rate constants vs. CPR concentration (see Figs. 8 and 9, which are published as supporting information on the PNAS web site). The pseudo-first-order rate constants were obtained from spectral changes at 415 nm at 15°C recorded on an OOBIBase32 instrument (Ocean Optics, Dunedin, FL.). The final concentrations of Fe(Schiff-base)·HO and NADPH were 5 and 100 μM, respectively, with aliquot addition of CPR (0.1, 0.15, 0.2, 0.25, and 0.3 μM), in 10 mM Tris·HCl (pH 7.4) at 15°C. The reaction was initiated by the addition of a buffer solution of Fe(Schiff-base)·HO (6.7 μM, 300 μl) to the mixture of CPR(0.4, 0.6, 0.8, 1.0, and 1.2 μM) and NADPH solution (400 μM, 100 μl) in an optical quartz cell.

Catalytic O_2 Reduction by Fe^{III}(Schiff-Base)·HO Composites. UV-vis spectral changes at 340 nm induced by NADPH consumption were recorded on an OOBIBase32 instrument (Ocean Optics). Oxygen consumption was measured by an oxygen electrode 9002SP (Toko Chemical Laboratories, Tokyo) and DO meter TD51 (Toko Chemical Laboratories) (see Fig. 10, which is published as supporting information on the PNAS web site). Each measurement was initiated with the addition of NADPH solution (final concentration: 100 μM in 10 mM Tris·HCl, pH 7.4) into the protein mixture solution [final concentrations of Fe(Schiff-base)·HO, CPR, and superoxide dismutase are 2 and 1 μM and 100 units, respectively, in 10 mM Tris·HCl buffer at pH 7.4 and 15°C] in a cuvette or an oxygen electrode cell (27). The NADPH and O_2 consumption rates were monitored at the initial stage during the catalytic reaction (Fig. 4) to exclude the influence of side reactions caused by excess H_2O_2.

Molecular Orbital Calculations. All calculations were carried out by using the GAUSSIAN03 program package (Revision B03) (39). We adopted x-ray crystallographic data for **1·HO**, **2·HO**, and **3·HO**. All hydrogen atoms were added by using HYPERCHEM (Release 6; Hypercube, Gainesville, FL) and relaxed by Amber molecular mechanics calculations (40, 41). The total charges of Fe(III) models of **1·HO**, **2·HO**, and **3·HO** are 0, 0, and +1, respectively. The Fe(III) and Fe(II) states were assumed high-spin (sextet) and low-spin (singlet), respectively.

The quality of the Gaussian type orbital basis functions used here is essentially identical to the valence double zeta plus single polarization level. For the Fe atom, we use the Huzinaga's (5333/53/5)[53321/53/41] set (42) plus *p*-type polarization function (a = 0.082), for C and N, the (63/5)/[621/41] set (42) plus *d*-type polarization function (a = 0.600) for C and (a = 0.864) for N. For O, the (63/5)/[621/41] set (42) plus *d*-type polarization function (a = 1.154) plus *p*-type anion basis (a = 0.059). For H, the (4)/[4] set (43) and H with hydrogen bonding, the (4)/[31] set [4] plus *p*-type polarization function (a = 1.0). The method is unrestricted Hartree–Fock.

All other experimental details are described in *Supporting Text*.

We thank Prof T. Yoshida (Yamagata University, Yamagata, Japan) for the gift of CPR; members of BL5 of Photon Factory for assistance during the diffraction data collection; Dr. Lipika Basumallic for assistance in preparation of the manuscript; and Prof. S. Aono for advice to redox potential measurements. This work was supported by Grants-in-Aid for Scientific Research 18685019 (to T.U.), 18770103 (to M.U.), 18370052 (to M.I.-S.), and on Priority Areas Chemistry of Coordination Space Grant 16074208 (to Y.W.) from the Ministry of Education, Culture, Sports, Science, and Technology (Japan), and the 21st Century Center of Excellence program of Nagoya University (to N.Y). Synchrotron radiation experiments were conducted under the approval of 2003G118 at Photon Factory. Portions of the x-ray diffraction data on the composites also were collected at the Hybrid Nano-Material Research Center of the Institute of Multidisciplinary Research for Advanced Materials, Tohoku University.

1. Pelletier, H. & Kraut, J. (1992) *Science* **258,** 1748–1755.
2. Tsukihara, T., Aoyama, H., Yamashita, E., Tomizaki, T., Yamaguchi, H., Shinzawa-Itoh, K., Nakashima, R., Yaono, R. & Yoshikawa, S. (1996) *Science* **272,** 1136–1144.
3. Ben-Shem, A., Frolow, F. & Nelson, N. (2003) *Nature* **426,** 630–635.
4. McLendon, G. & Hake, R. (1992) *Chem. Rev.* **92,** 481–490.
5. Nocek, J. M., Zhou, J. S., DeForest, S., Priyadarshy, S., Beratan, D. N., Onuchic, J. N. & Hoffman, B. M. (1996) *Chem. Rev.* **96,** 2459–2489.
6. Gray, H. B. & Winkler, J. R. (1996) *Annu. Rev. Biochem.* **65,** 537–561.
7. Heller, A. (1990) *Acc. Chem. Res.* **23,** 128–134.
8. Willner, I. & Katz, E. (2000) *Angew. Chem. Int. Ed.* **39,** 1180–1218.
9. Armstrong, F. A. & Wilson, G. S. (2000) *Electrochim. Acta* **45,** 2623–2645.
10. Xiao, Y., Patolsky, F., Katz, E., Hainfeld, J. F. & Willner, I. (2003) *Science* **299,** 1877–1881.
11. Hayashi, T., Hitomi, Y. & Ogoshi, H. (1998) *J. Am. Chem. Soc.* **120,** 4910–4915.
12. Hu, Y. Z., Tsukiji, S., Shinkai, S., Oishi, S. & Hamachi, I. (2000) *J. Am. Chem. Soc.* **122,** 241–253.
13. Dunn, A. R., Dmochowski, I. J., Winkler, J. R. & Gray, H. B. (2003) *J. Am. Chem. Soc.* **125,** 12450–12456.
14. Benson, D. E., Conrad, D. W., de Lorimer, R. M., Trammell, S. A. & Hellinga, H. W. (2001) *Science* **293,** 1641–1644.
15. Chu, G. C., Katakura, K., Zhang, X. H., Yoshida, T. & Ikeda-Saito, M. (1999) *J. Biol. Chem.* **274,** 21319–21325.
16. Vermilion, J. L. & Coon, M. J. (1978) *J. Biol. Chem.* **253,** 8812–8819.
17. Wang, J. L. & Ortiz de Montellano, P. R. (2003) *J. Biol. Chem.* **278,** 20069–20076.
18. Ohashi, M., Koshiyama, T., Ueno, T., Yanase, M., Fujii, H. & Watanabe, Y. (2003) *Angew. Chem. Int. Ed.* **42,** 1005–1008.
19. Ueno, T., Ohashi, M., Kono, M., Kondo, K., Suzuki, A., Yamane, T. & Watanabe, Y. (2004) *Inorg. Chem.* **43,** 2852–2858.
20. Ueno, T., Koshiyama, T., Ohashi, M., Kondo, K., Kono, M., Suzuki, A., Yamane, T. & Watanabe, Y. (2005) *J. Am. Chem. Soc.* **127,** 6556–6562.
21. Hirotsu, S., Chu, G. C., Unno, M., Lee, D. S., Yoshida, T., Park, S. Y., Shiro, Y. & Ikeda-Saito, M. (2004) *J. Biol. Chem.* **279,** 11937–11947.
22. Hunter, C. L., Lloyd, E., Eltis, L. D., Rafferty, S. P., Lee, H., Smith, M. & Mauk, A. G. (1997) *Biochemistry* **36,** 1010–1017.
23. Schuller, D. J., Wilks, A., Ortiz de Montellano, P. R. & Poulos, T. L. (1999) *Nat. Struct. Biol.* **6,** 860–867.
24. Sugishima, M., Omata, Y., Kakuta, Y., Sakamoto, H., Noguchi, M. & Fukuyama, K. (2000) *FEBS Lett.* **471,** 61–66.
25. LaMar, G. N., Toi, H. & Krishnamoorthi, R. (1984) *J. Am. Chem. Soc.* **106,** 6395–6401.

26. Zeng, Y., Deshmukh, R., Caignan, G. A., Bunce, R. A., Rivera, M. & Wilks, A. (2004) *Biochemistry* **43,** 5222–5238.
27. Liu, Y., Moenne-Loccoz, P., Hildebrand, D. P., Wilks, A., Loehr, T. M., Mauk, A. G. & Ortiz de Montellano, P. R. (1999) *Biochemistry* **38,** 3733–3743.
28. Davies, A. M., Guillemette, J. G., Smith, M., Greenwood, C., Thurgood, A. G. P., Mauk, A. G. & Moore, G. R. (1993) *Biochemistry* **32,** 5431–5435.
29. Munro, A. W., Noble, M. A., Robledo, L., Daff, S. N. & Chapman, S. K. (2001) *Biochemistry* **40,** 1956–1963.
30. Goto, Y., Watanabe, Y., Fukuzumi, S., Jones, J. P. & Dinnocenzo, J. P. (1998) *J. Am. Chem. Soc.* **120,** 10762–10763.
31. Jones, R. D., Summerville, D. A. & Basolo, F. (1979) *Chem. Rev.* **79,** 139–179.
32. Proniewicz, L. M., Isobe, T. & Nakamoto, K. (1989) *Inorg. Chim. Acta* **155,** 91–94.
33. Wang, J., Evans, J. P., Ogura, H., Mar, G. N. L. & Ortiz de Montellano, P. R. (2006) *Biochemistry* **45,** 61–73.
34. Roitberg, A. E., Holden, M. J., Mayhew, M. P., Kurnikov, I. V., Beratan, D. N. & Vilker, V. L. (1998) *J. Am. Chem. Soc.* **120,** 8927–8932.
35. Koopmans, T. (1934) *Physica* **1,** 104–113.
36. Babini, E., Bertini, I., Borsari, M., Capozzi, F., Luchinat, C., Zhang, X. Y., Moura, G. L. C., Kurnikov, I. V., Beratan, D. N., Ponce, A., *et al.* (2000) *J. Am. Chem. Soc.* **122,** 4532–4533.
37. Olivas, E., Dewaal, D. J. A. & Wilkins, R. G. (1977) *J. Biol. Chem.* **252,** 4038–4042.
38. Oprian, D. D., Vatsis, K. P. & Coon, M. J. (1979) *J. Biol. Chem.* **254,** 8895–8902.
39. Frisch, M. J., Trucks, G. W., Schlegel, H. B., Scuseria, G. E., Robb, M. A., Cheeseman, J. R., Montgomery, J., J. A., Vreven, T., Kudin, K. N., Burant, J. C., *et al.* (2004) GAUSSIAN03 (Gaussian, Wallingford, CT), Revision B03.
40. Weiner, S. J., Kollman, P. A., Case, D. A., Singh, U. C., Ghio, C., Alagona, G., Profeta, S. & Weiner, P. (1984) *J. Am. Chem. Soc.* **106,** 765–784.
41. Weiner, S. J., Kollman, P. A., Nguyen, D. T. & Case, D. A. (1986) *J. Comput. Chem.* **7,** 230–252.
42. Huzinaga, S., Andzelm, J., Klobukowski, M., Radzio-Andzelm, E., Sakai, E. & Takewaki, H. (1984) *Gaussian Basis Set for Molecular Calculation* (Elsevier, New York).
43. Huzinaga, S. (1965) *J. Chem. Phys.* **42,** 1293–1302.